Probing the high redshift universe with hyperfine transition of ^{3}He II

J. S. Bagla

Harish-Chandra Research Institute, Allahabad

jasjeet@hri.res.in

Cosmological Reionization @ HRI

Feb.19, 2010

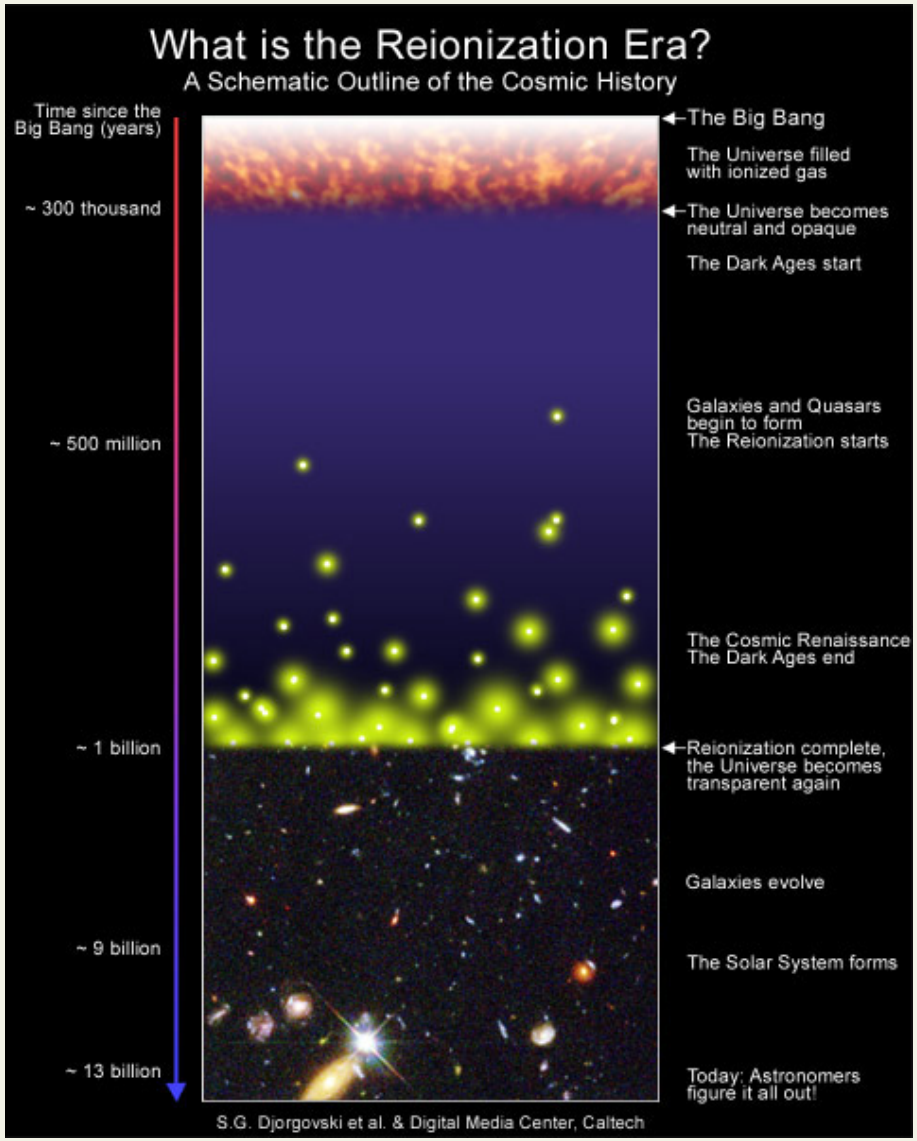

Figure 1: Reionization of the universe. Credit & Copyright: LOFAR EoR team.

Hyperfine structure of electronic states in atoms arises due to the interaction of the magnetic moment of the nucleus and electron(s).

$$\langle H_1 \rangle = \frac{4}{3} g_N \frac{m}{M_n} (Z\alpha)^4 mc^2 \frac{1}{n^3} \frac{(\mathbf{S}.\mathbf{I})}{\hbar^2} \quad ; \qquad l = 0$$

For Hydrogen, this leads to a splitting of the ground state. The new ground state is a singlet and the excited state is a triplet.

The difference of energy in two states is very small, smaller than that caused in typical energy levels by the fine structure, hence the name *Hyperfine* transition.

Two processes couple T_s and T_{kin}: slow (atom-atom and atom-electron) collisions leading to randomization of spin (Purcell & Field, 1956; Field, 1958), and, Lyman series photons (Wouthuysen, 1952; Field, 1958; Hirata, 2006).

$$T_s^{-1} = \frac{T_{cmb}^{-1} + T_{\rm kin}^{-1} x_c + T_\alpha^{-1} x_\alpha}{1 + x_c + x_\alpha}$$

Here x_c, the collisional coupling efficiency is proportional to the ratio of radiative decay time and mean time between collisions.

These couplings ensure that T_s lies between T_{kin} and T_{cmb}. Collisional coupling is not very strong, except inside collapsed haloes or overdense regions with significant ionized fraction where electron–atom collisions play a dominant role.

Lyman series photons are abundant, except in the early stages of EoR, and we get $T_S \simeq T_{kin}$. Patchiness in the Lyman series photon distribution can be probed using radiation in this transition (Barkana & Loeb, 2005).

Observable quantity is the brightness temperature:

$$\delta T_b(z) = 4.6mK \left(1 - \frac{T_{cmb}}{T_s}\right) x_{HI} \left(1 + \delta_{gas}\right) (1+z)^2 \frac{H_0}{H(z)} \left[\frac{H(z)}{(1+z)(dv_{\parallel}/dr_{\parallel})}\right]$$

where T_{cmb} is the CMBR temperature at the appropriate redshift.

Motions can change the frequency spread of the spectral lines.

If $T_s \gg T_{cmb}$, the emission in this transition is independent of the gas temperature.

$$\delta T_b(z) = 4.6mK \quad x_{HI} \left(1 + \delta_{gas}\right) (1+z)^2 \frac{H_0}{H(z)} \left[\frac{H(z)}{(1+z)(dv_{\parallel}/dr_{\parallel})}\right]$$

Hyperfine transition of ^{3}He II is also a potential probe of the high redshift universe (JSB & Loeb, 0905.1698; McQuinn & Switzer, 0905.1715).

Rest frame frequency of the transition is 8.67 GHz. Abundance of ^{3}He is a little more than 10^{-5} relative to Hydrogen.

$T_\star = h\nu/k_B = 0.42$ K. In this case, the excited state is the singlet and the ground state is the triplet: $(g_1/g_0) = 1/3$.

The Einstein coefficient for this transition is $A_{21} = 1.96 \times 10^{-12}\mathrm{s}^{-1}$, this is 600 times larger than the corresponding coefficient for neutral hydrogen.

Ionization potential for Hydrogen is 13.6 eV, ionization potential for Helium is 24.6 eV for the first electron and 54.4 eV for the second electron.

Expected signal is weak compared to the signal expected from H I, but the level of difficulty in detection does not differ by orders of magnitude.

The radiative decay time is much shorter than that for H I. This leads to a much weaker efficiency for collisional coupling of the spin temperature and the gas temperature.

Gas temperature in regions with ^{3}He II is typically high, several thousands of degrees. Thus even a weak coupling can potentially lead to a spin temperature that is well above the CMB temperature.

This transition can never be seen in absorption against the CMB.

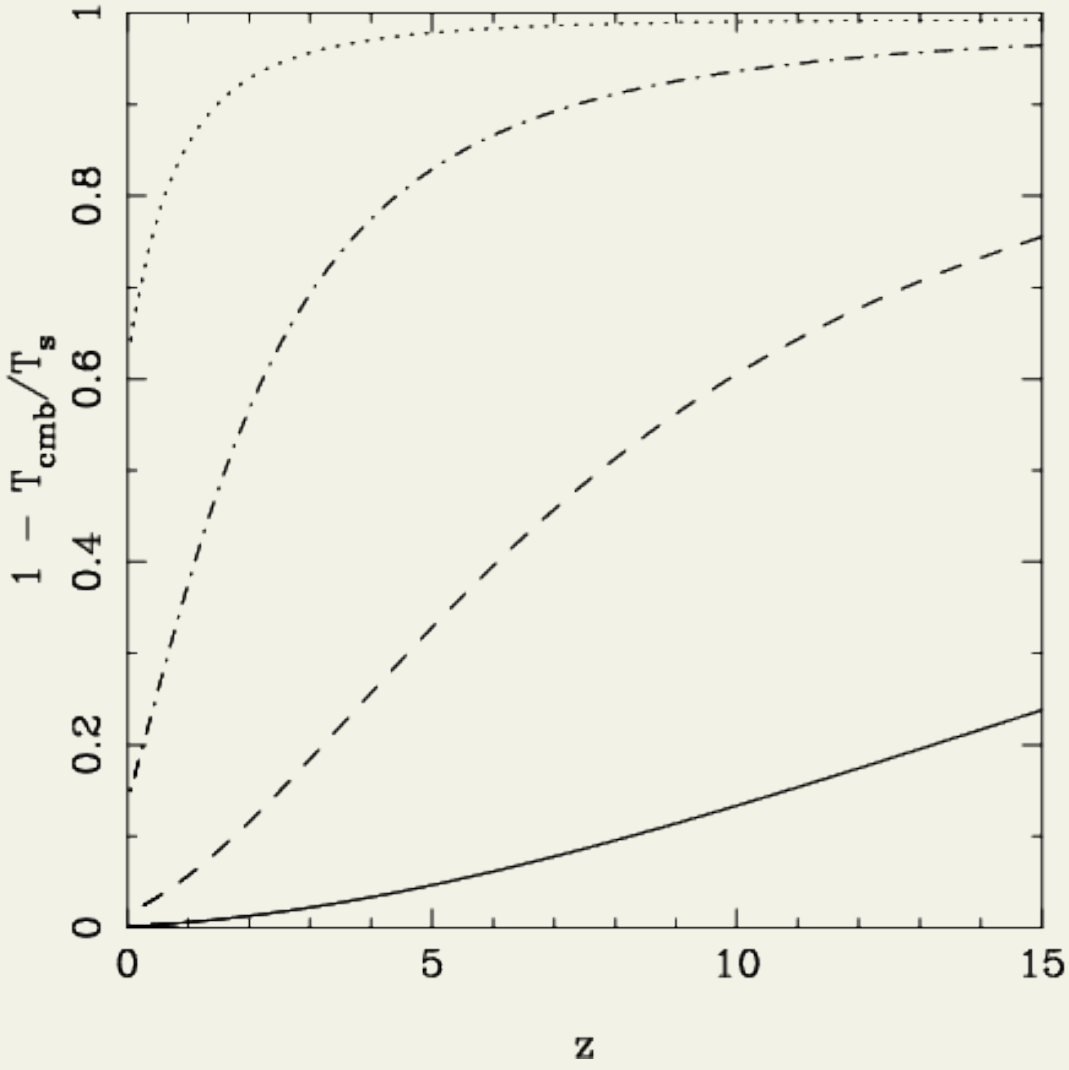

Figure 2: Expected spin temperature for regions with different overdensity as a function of redshift (Bagla & Loeb, 2009).

The expected absorption signal is:

$$\tau_\nu = \frac{1}{32\pi}\frac{hc^3 A_{10}}{k_B T_s \nu_0^2}\frac{x_{HeII} n_{^3He}}{(1+z)(dv_\parallel/dr_\parallel)}$$

This is of considerable interest for studying ^{3}He II reionization around $z \sim 3$ (McQuinn & Switzer, 2009).

$$\tau_\nu = 4.4\times10^{-6} \quad \frac{x_{HeII}}{T_s/T_{cmb}(z)}\frac{(1+\delta)}{10}\left(\frac{1+z}{4}\right)^{3/2}\left(\frac{n_{^3He}/n_H}{1.1\times10^{-5}}\right)\left[\frac{H(z)}{(1+z)\left(\frac{dv_\parallel}{dr_\parallel}\right)}\right]$$

Optical depth is small and requires that the spin temperature be small. Cross-correlating with Lyman-α forest will help to improve S/N. Detection potentially possible with $50-100$ hours with the GBT (McQuinn & Switzer, 2009).

Absorption depends on the local density through spin temperature as well.

Fluctuations in x_{HeII} also contribute, hence will depend on fluctuations in the UVB around 54 eV.

Absorption by DLAS is a possibility.

The contribution of the warm neutral phase of the ISM is suppressed due to a small x_{HeII} and a high T_s. Overdensity in this phase is fairly high.

The contribution of the warm ionized phase of the ISM is suppressed due to a higher T_s. In this phase x_{HeII} is expected to be close to unity, though density is much lower than the warm neutral medium.

Absorption studies of the Lyman-α forest can potentially put constraints on BBN.

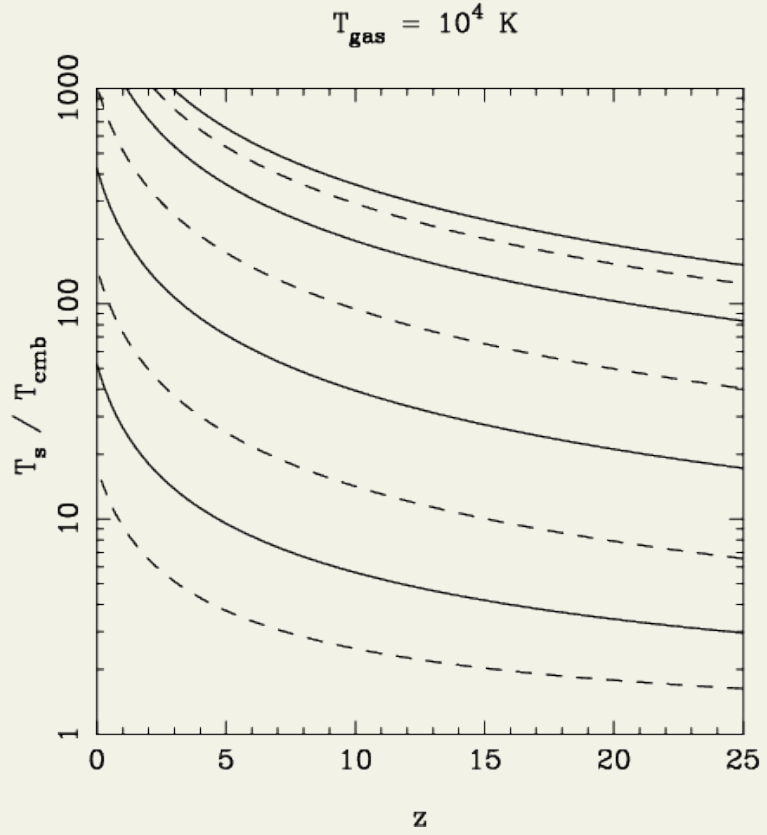

Figure 3: Expected spin temperature for regions with different electron number density. Curves are for $n_e = 10^{-2}$, 0.1, 1 and 10 per cc. Kinetic temperature is assumed to be 10^4 K. Solid lines are for the Goss & Goldwire (1967) estimate of collisional coupling, and dashed lines are for the McQuinn & Switzer (2009) estimate.

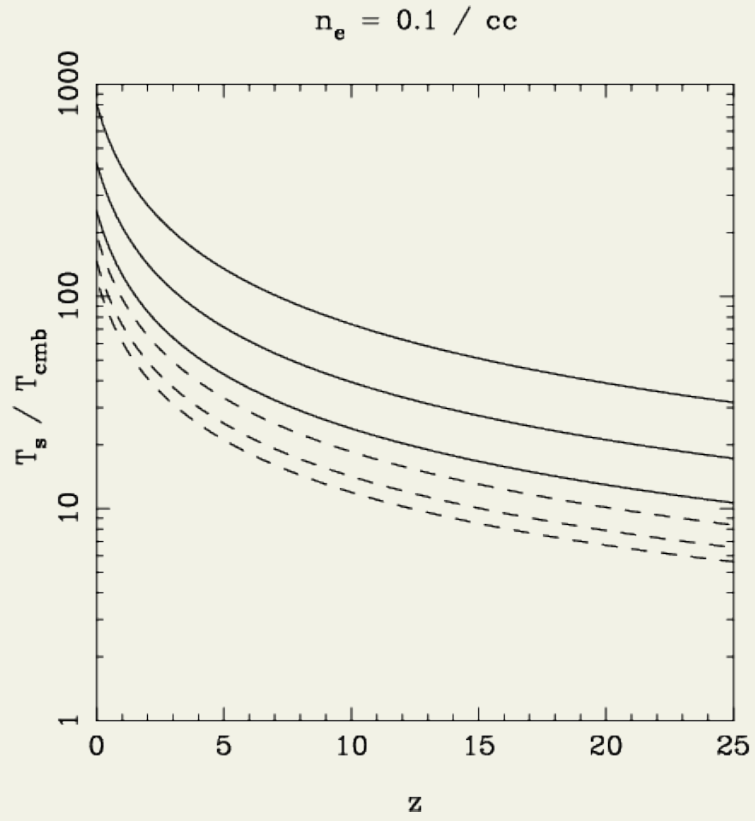

Figure 4: Expected spin temperature for regions with different electron number density. Curves are for $T_{gas} = 20000$, 10000 and 5000 K. Electron number density is assumed to be 0.1 /cc. Solid lines are for the Goss & Goldwire (1967) estimate of collisional coupling, and dashed lines are for the McQuinn & Switzer (2009) estimate.

Emission from the EoR is small.

$$\delta T_b = 20\mu\mathrm{K}\ x_{HeII}\left(1-\frac{T_{cmb}}{T_s}\right)\left[\frac{1+\delta}{10}\right]\left[\frac{1+z}{11}\right]^{1/2}\left(\frac{n_{^3He}/n_H}{1.1\times10^{-5}}\right)\left[\frac{H(z)}{(1+z)\left(\frac{dv_\parallel}{dr_\parallel}\right)}\right]$$

Except for sources with a hard spectrum (stars much more massive than 100 $\mathrm{M}_\odot$, or AGNs), x_{HeII} in cosmological H II regions is close to unity.

T_{cmb}/T_s is around 0.4 for $1+\delta\sim10$ at $z\simeq10$, and is smaller for higher density regions.

Due to higher rest frame frequency, $T_{sys} > T_{sky}$ up to $z_{em}\sim25$. In comparison, we enter the sky dominated regime at $z_{em}\sim5$ for H I emission.

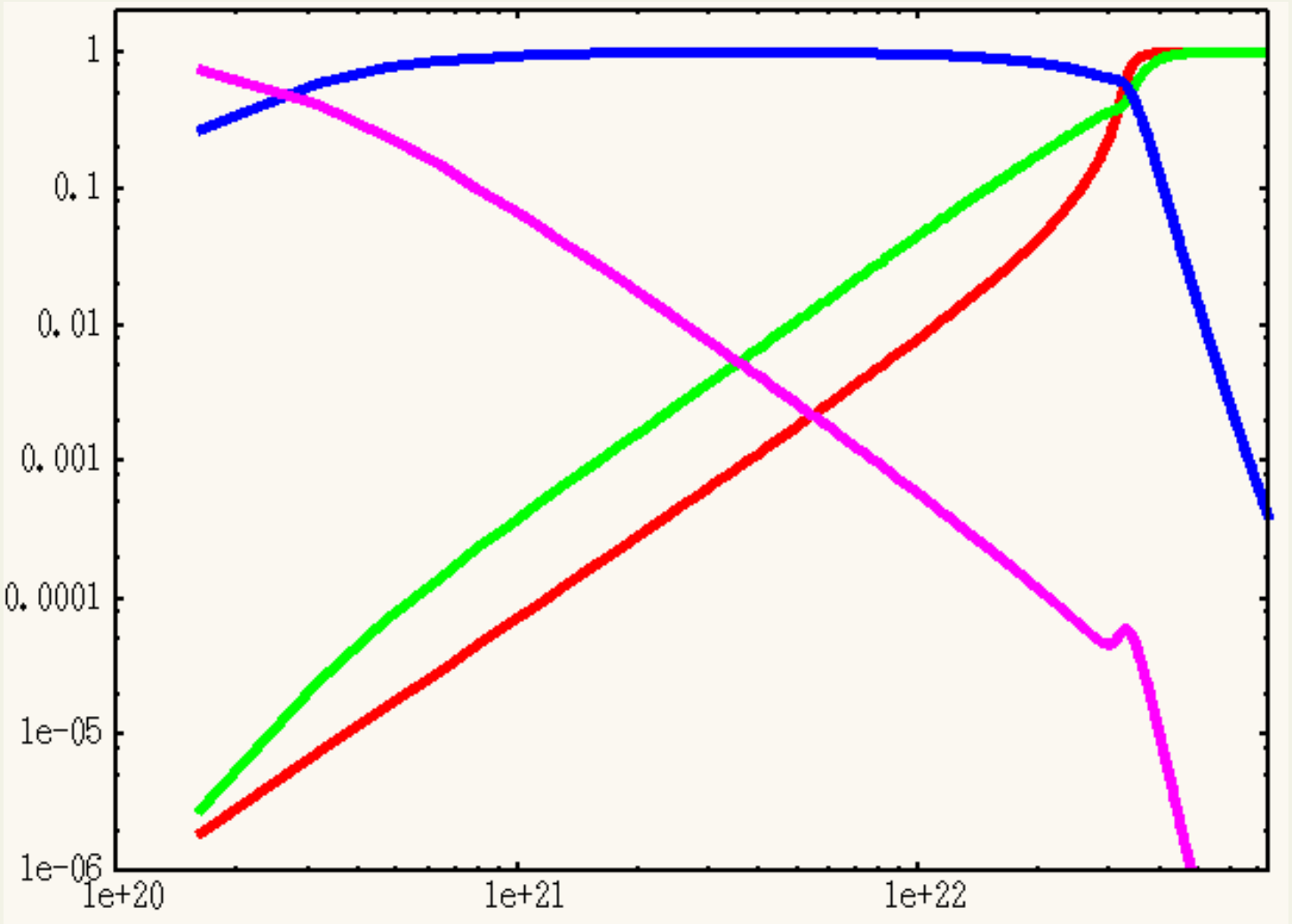

Figure 5: H I (red), He I (green), He II (blue) and He III (purple) distribution around a black-body source with $T_{eff} = 10^4$ K and ionizing luminosity 10^6 $L_\odot$.

Thus ^{3}He II signal from the epoch of reionization can complement the H I signal.

The ^{3}He II fraction depends on the ionizing spectrum. Thus the signal from this transition can be used to constrain the mix of sources that were responsible for reionization.

Stronger sources can fully ionize Helium but at $z \geq 7$ it recombines over a short time scale to ^{3}He II . Thus the signal from his transition is likely to vary more strongly with time as power sources like AGNs switch on/off.

Ly-α blobs are amongst the most promising sources. These blobs are tens of kpc across and contain gas at a high overdensity.

$$\delta T_b = 120\mu\mathrm{K}\ x_{HeII}\left(1-\frac{T_{cmb}}{T_s}\right)\left[\frac{1+\delta}{100}\right]\left[\frac{1+z}{4}\right]^{1/2}\left(\frac{\frac{n_{3\,He}}{n_H}}{1.1\ \ 10^{-5}}\right)\left[\frac{H(z)}{(1+z)\left(\frac{dv_\parallel}{dr_\parallel}\right)}\right]$$

Uncertainty in the signal arises largely from the velocity factor: if the Lyman-α blobs contain emitting regions within the virialized halo then that can suppress the signal by a factor of 5 or so.

Discovered a decade ago (Keel et al, 1999; Steidel et al, 2000), these are seen over a range of redshifts: $6 \geq z \geq 2$. Hundreds of blobs have been discovered (see Yamada, 2009 for an overview).

There are three potential sources of energy in these blobs: AGN/Starburst, Mechanical heating by winds, Gravitational collapse. The last category, identified with formation of massive galaxies, is of greater interest to us.

It is possible to observe the signal from typical sources with existing telescopes like the GBT with a few hundred hours of observations (JSB, Kanekar & Loeb, GBT proposal). Prospects are enhanced as there are fields with multiple blobs.

Due to RFI, we changed the target region after 12 hours of observations. Our first choice for target was the Subaru group of Lyman-α blobs at $z = 3.1$. We are now targeting a Lyman-α blob at $z = 2.83$ discovered by Smith & Jarvis (2007).

In the post-reionization era, H I exists only in galaxies, which in turn live in highly overdense haloes.

Further, the haloes must contain enough gas to self shield from the UV background. This requires $v_{circ} \geq 30$ km/s (Pontzen et al. 2008) at $z \sim 3$.

If the haloes are too massive then the virial temperature of gas is very high and gas cannot cool. This happens for haloes with $v_{circ} \gg 200$ km/s (Pontzen et al. 2008).

Neutral gas at high redshifts is known to have a fairly high spin temperature (Kanekar et al. 2009).

Total amount of H I at high redshifts ($5 \geq z \geq 1$) is also well constrained with $\Omega_{HI} \simeq 0.001$ (Péroux et al. 2005).

We use large N-Body simulations, done with 10^8 particles to model the large scale structure of the universe at high redshifts.

At each redshift of interest, we ensure that we resolve the smallest haloes that contain significant amount of H I. This is done by choosing the mass of each N-Body particle to be around $1/10$ of this minimum halo mass.

We demonstrate that the size of the simulation box is large enough so that the contribution of perturbations at larger scales to the statistical signal is ignorable (below 10%).

We identify dark matter haloes of all masses in the simulation output. H I is then assigned to these haloes in such a way that the H I fraction is suppressed for haloes with $v_c \geq 200$ km/s.

We do not assign any H I to haloes with mass below the minimum threshold described above.

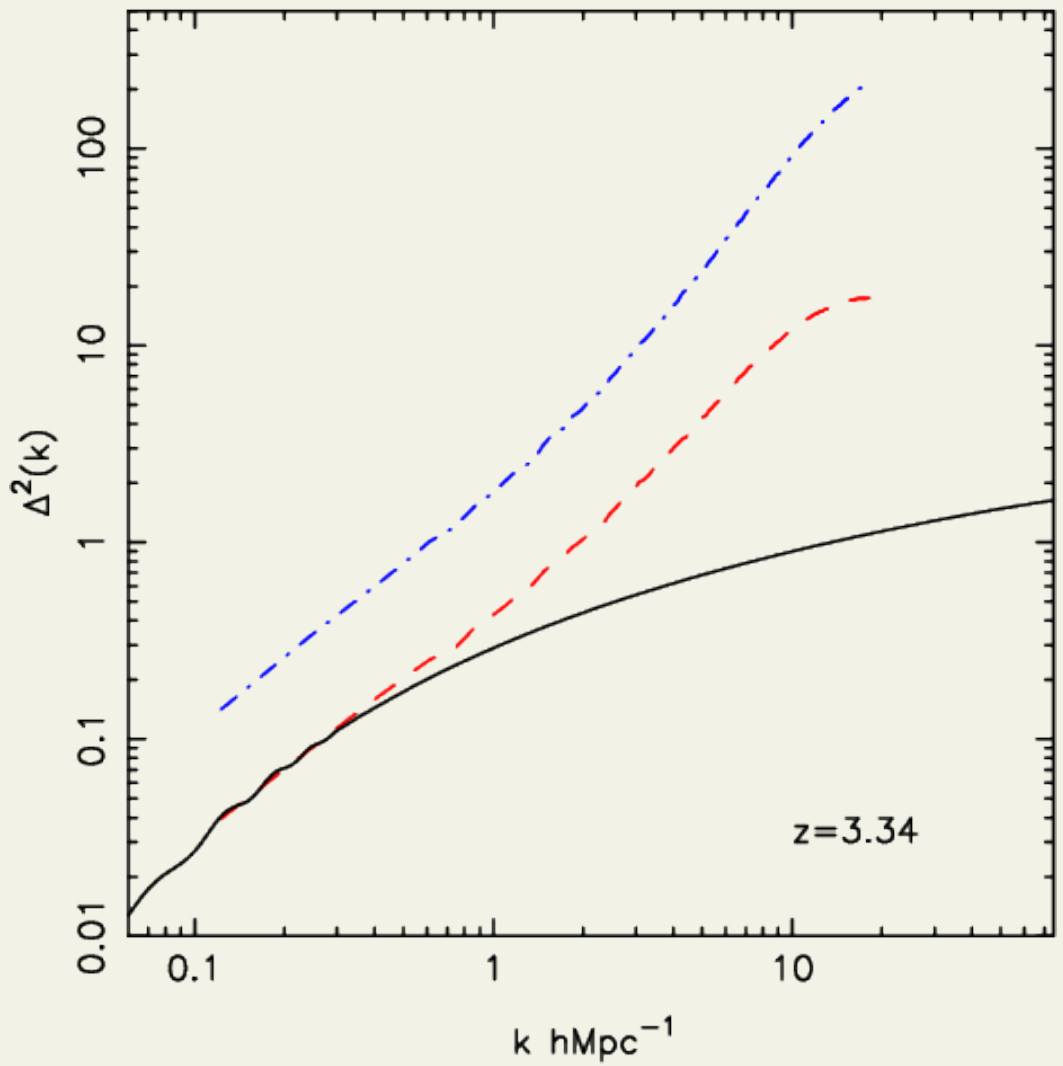

Figure 6: The linear, the non-linear and the H I power spectrum at $z = 3.34$. JSB & Khandai (0908.3796).

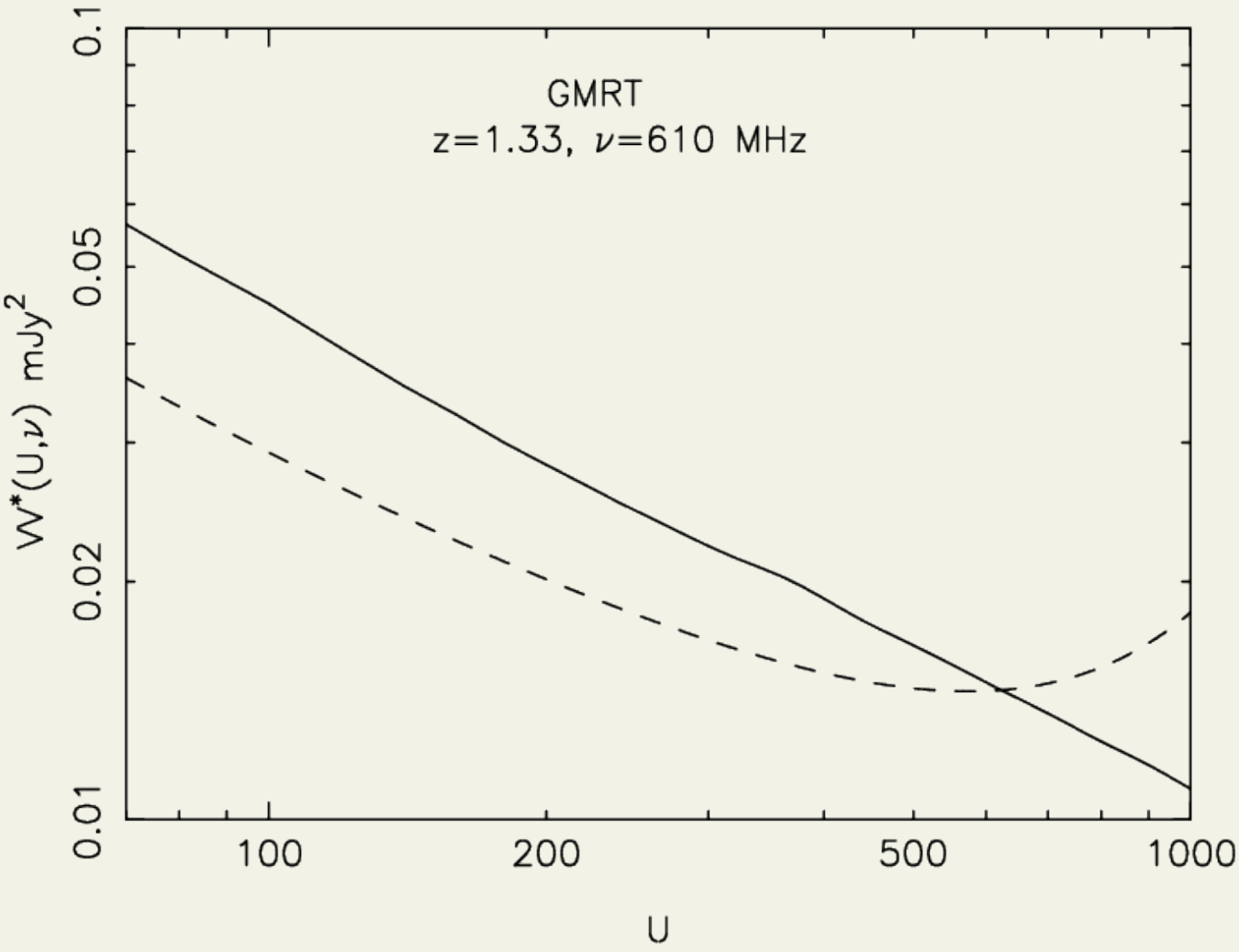

Figure 7: Visibility correlations. Khandai, Datta & JSB (0908.3857).

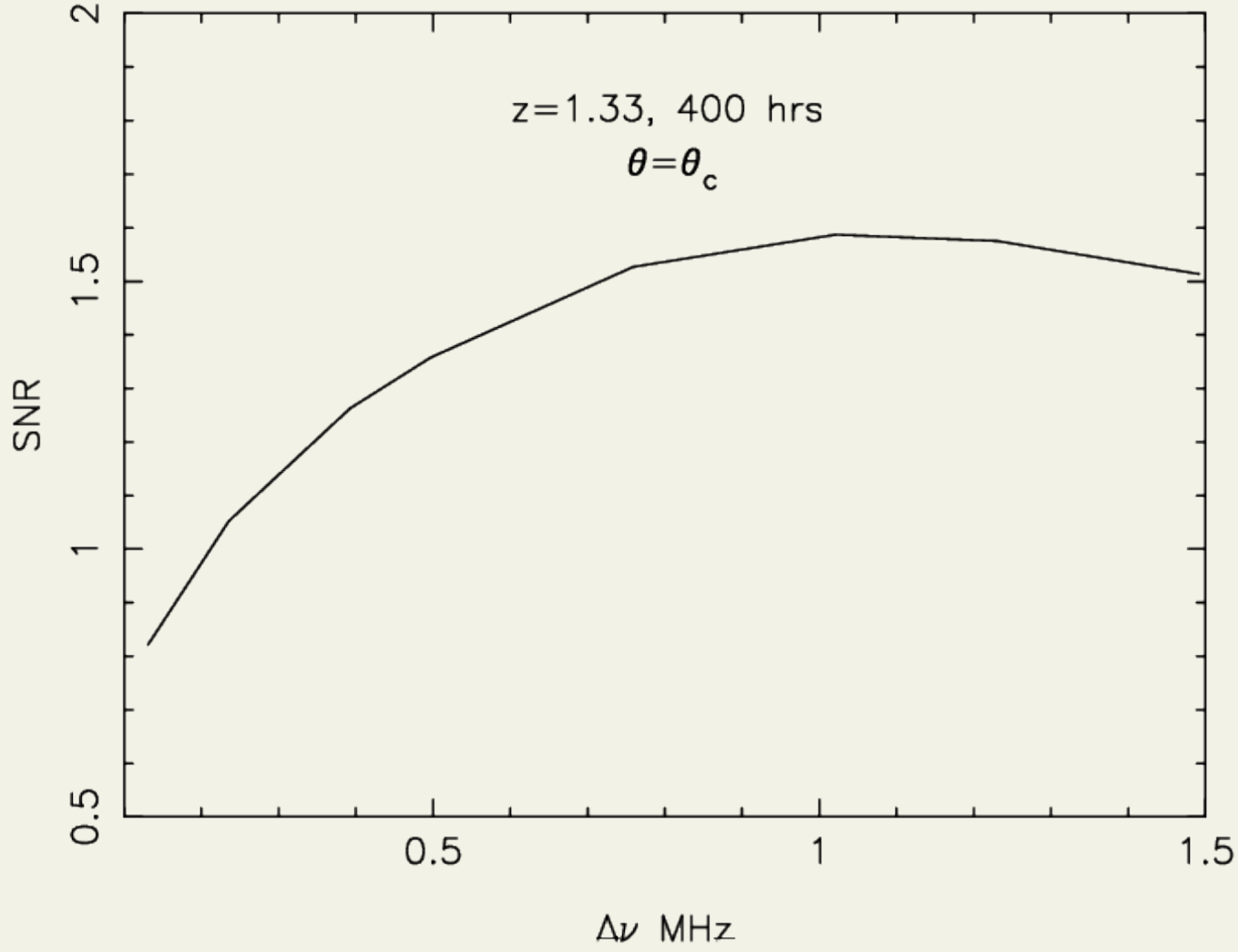

Figure 8: Signal to noise ratio for rare peaks in signal. Khandai, Datta & JSB (0908.3857).

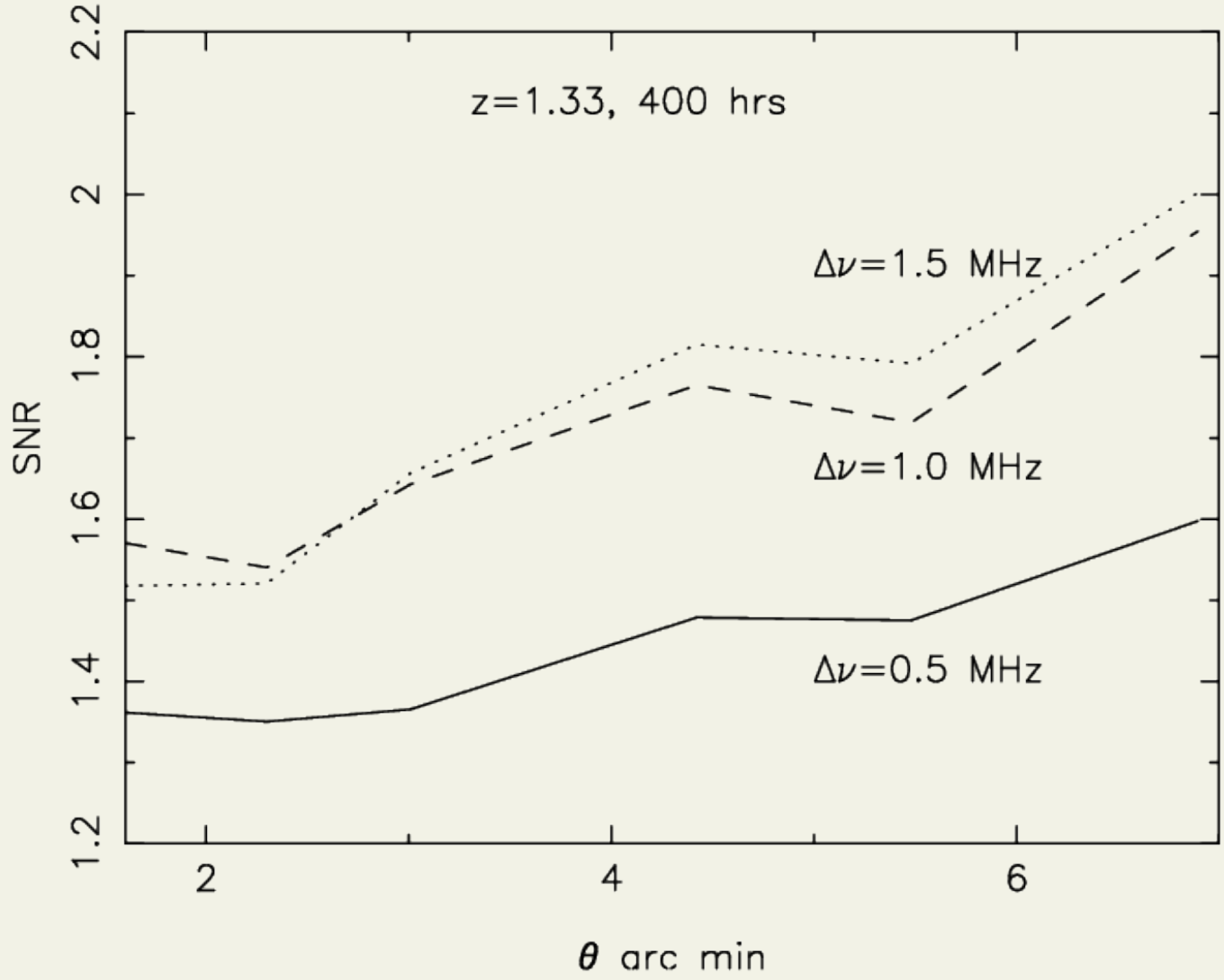

Figure 9: Signal to noise ratio for rare peaks in signal. Khandai, Datta & JSB (0908.3857).

Hyperfine transitions of H I and ^{3}He II are important probes of the IGM and the epoch of reionization.

In view of upcoming radio telescopes, it is important to understand the physical processes that are responsible for evolution of H I and ^{3}He II .

Enhancement in clustering of H I at small scales is a significant feature and we should exploit this to design upcoming surveys.

^{3}He II is a potential probe of the high redshift universe, and can be used to obtain complementary information as compared to the radiation from H I. It is eminently observable, and first detection from a cosmological source should be possible in coming years. More detailed modeling is required.

Collaborators: Kanan Datta (LOFAR/Stockholm University), Nissim Kanekar (NCRA), Nishikanta Khandai (CMU), Girish Kulkarni (HRI), Avi Loeb (CfA, Harvard) & Jaswant Yadav (HRI).